Proceedings of the ASME 2010 3rd Joint US-European Fluids Engineering Summer Meeting and 8th International Conference on Nanochannels, Microchannels, and Minichannels
FEDSM-ICNMM2010
August 1-5, 2010, Montreal, Canada

FEDSM-ICNMM2010-31131

HEAT TRANSFER EXPERIMENTS OF ETHYLENE GLYCOL-WATER MIXTURE IN MULTI-PORT SERPENTINE MESO-CHANNEL HEAT EXCHANGER SLAB

Mesbah G. Khan
Mechanical, Automotive and Materials Engineering
University of Windsor,
Windsor, N9B 3P4, Ontario, Canada
Khan13j@uwindsor.ca; mesbah_khan@hotmail.com

Amir Fartaj*
Mechanical, Automotive and Materials Engineering
University of Windsor,
Windsor, N9B 3P4, Ontario, Canada
fartaj@uwindsor.ca*

ABSTRACT

In past few years, narrow diameter flow passages (≤3 mm) have attracted huge research attentions due to their several advantageous features over conventional tubes (≥6 mm) especially from the view points of higher heat transfer, lesser weight, and smaller device size. Several classifications of narrow channels, based on sizes, are proposed in the open literature from mini to meso and micro (3 mm to 100 μm). The meso- and micro-channels have not yet entered into the HVAC and automotive heat exchanger industries to the expected potentials to take the above-mentioned advantages. The reasons may be the limited availability of experimental data on pressure drop and heat transfer and the lack of consolidated design correlations as compared to what is established for compact heat exchangers. While a number of studies available on standalone single straight channels, works on multi-channel slab similar to those used as typical thermal heat exchanger core elements are inadequate, especially the research on multi-channel serpentine slab are limited in the open literature. The 50% ethylene glycol and water mixture is widely used in heat exchanger industry as a heat transfer fluid. Studies of pressure drop and heat transfer on this commercially important fluid using narrow tube multi-channel slab is scarce and the availability of experimental data is rare in the open literature. Conducting research on various shapes of meso- and micro-channel heat exchanger cores using a variety working fluids are a definite needs as recommended and consistently urged in ongoing research publications in this promising area.

Under present long-term project, an automated dynamic single-phase experimental infrastructure has been developed to carryout the fluid flow and heat transfer research in meso- and micro-channel test specimens and prototype microchannel heat exchanger using a variety of working fluids in air-to-liquid crossflow orientation. In the series, experiments have been conducted on 50% ethylene glycol and water solution in a serpentine meso-channel slab having 68 individual channels of 1 mm hydraulic diameter to obtain the heat transfer data and the general pressure drop nature of the test fluid. Current paper presents the heat transfer characteristics of ethylene glycol-water mixture and the Reynolds number effects on pressure drop, heat transfer rate, test specimen NTU and effectiveness, overall thermal resistance, and the Nusselt number.

INTRODUCTION

Heat exchangers have wide applications in industries e.g. building, HVAC, energy, transportation, automotive to name a few. They use a variety of flow passages and a number of heat transfer fluids. Achieving high heat transfer using miniaturized unit has become a progressive demand among the industries. Small flow passages (≤3 mm) represent the next steps in heat exchanger development due to holding high heat transfer, light-weight, and space minimizing potentials over traditional tubes (≥6 mm). Researchers are working on narrow passages with various shapes and orientations.

Majority of the studies on narrow diameter tubes available in the literature used straight and standalone single port narrow-channel. Many of the earlier works reported contradictory heat transfer and fluid flow results. Some of the results could be predicted using traditional correlations and some were either lower or higher than or very different from the traditional theory, which can be found in some published works such as by Steinke and Kandlikar (2006) and Morini (2004) [1-2]. Additional information, recommendations and updates on heat transfer and fluid flow in microchannels are available in published work by Kandlikar et al. (2006) [3].

Single-phase heat transfer and fluid flow have many practical interests for example in automotive and fuel cell heat exchangers among other applications. According to Steinke and

Kandlikar (2004) a single-phase narrow tube system can chase a two-phase flow heat exchange device and can simplify the overall necessity of complex two-phase device [4]. Khan et al. (2010) found that the heat transfer rates per unit volume and surface area, effectiveness, and the number of transfer unit are all improved when narrow-channel slab is used as a heat exchanger core place of either elliptical or circular tubes [5]. The increased number of channels in multi-port tubing increases both the heat transfer as well as the pressure drop; the circular cross-section provides overall the best thermal and hydrodynamic performances over other geometries [6].

The multi-port straight or serpentine flat slabs with or without fins are frequently encountered as the cores in many typical heat exchangers. Studies on these applied geometries are found relatively less in the literature. Some works are found [7-11] to report the heat transfer and fluid flow results in narrow size multi-port slabs but the test specimens used in these studies were standalone straight, non-circular, and un-finned. While some works on microchannel heat exchangers or heat sinks using non-circular cross-section are available, such as [12-17], the detailed study on a complete heat exchanger made of narrow diameter circular channels is still insufficient.

Research on various liquid working fluids in narrow channel heat exchangers in general, and on viscous liquids in particular, is also limited in the literature. A viscous working fluid often experiences laminar flow regime and longer flow developing length depending on the operating condition. Research on viscous fluids in narrow channel heat exchanger is important in order to properly account for the fluid flow and heat transfer correlations. The ethylene glycol-water solution is widely used in heat exchanger industry as the heat transfer fluid. Study on this commercially important fluid in meso- and micro-channels is scarce and the availability of experimental data is rare in the open literature. Garimella et al. (2001) in single tube and Jokar et al. (2009) in complete heat exchanger both investigated glycol-water mixture flow using non-circular cross-section [7, 17]. The hydraulic diameters used were from 1.74-3.02 mm (Garimella) and from 2.60-4.1 mm (Jokar), all of which are higher than the size chosen in current study.

The channel diameter and the flow length together also determine whether the flow is fully developed or developing. This is particularly true when the channel length-to-diameter ratio has a finite small value as is the case for typical automotive heater core. In developing flow the heat transfer coefficient at the channel entrance is higher than the channel exit and the average heat transfer coefficient is higher than the fully developed values [7]. The temperature dependency of thermophysical properties of working fluids could be important in developing flow [18]. The presence of serpentine or flow reversal bend in a heat exchanger core may pose additional entrance effects thereby increasing both the heat transfer and the flow resistance [19-20]. In such situation the flow may or may not achieve the fully developed status before exiting the core. Works on thermally or simultaneously developing laminar flow in narrow channel straight or serpentine test samples are also rare. Research on these aspects is very important because of the fact that the accurate prediction of tube-side heat transfer and pressure drop mechanisms in developing flow are also the essential key to the heat exchanger design and sizing.

It can be summarized that the research on multi-port circular narrow channel test specimens and on complete heat exchanger in serpentine configuration is rare. Conducting research on various shapes of meso- and micro-channel heat exchanger cores using a variety of working fluids is thus a definite need, which is constantly urged by ongoing research publications in this promising area. Therefore, a long-term research project has been undertaken by the authors to conduct the heat transfer and fluid flow experiments on meso-channel test specimens and on heat exchanger. The objectives of the research are to obtain the heat transfer and pressure drop experimental data and correlations of various working fluids in the test samples. To fulfill the objectives, a dynamic liquid-to-air cross-flow experimental facility has been developed and several meso-size test specimens and a heat exchanger have been designed. Each sample is unique in profile and has not been studied before.

In the ongoing series, experiments have been conducted on MCHX#4, which is a finned and serpentine circular multi-port flat slab having 68 channels of 1 mm in diameter each. The 50% ethylene glycol-water mixture was tested as the working fluid in developing laminar flow regime in the Reynolds number range between 400 and 1800. Current paper presents the pressure drop behavior and the heat transfer characteristics of the ethylene-glycol water mixture in terms of Reynolds number effects on the heat transfer rate, test slab NTU and effectiveness, overall thermal resistance and Nusselt number. Other investigations in the series are in progress.

EXPERIMENTAL SETUP AND TEST PROCEDURES

A large research group in this area focused on internal fluid and therefore used test facilities where test specimens were externally heated by electrical means. Test facility where both working fluids are in motion is limited in the open literature. This area lacks the established guidelines and standard procedures on how to set up an experimental facility for heat and fluid flow research in narrow channels. Steinke et al. (2006) however provided some useful information [21]. A liquid-to-air single-phase crossflow dynamic test facility has been developed for present study as illustrated in Fig. 1. It is capable to provide with fluid flow and heat transfer research facilities on different microchannel geometries using various liquid working fluids in a broad range of flow, pressure and temperature condition. Attentions are paid to the high accuracy instruments, key system components, and data monitoring and acquisition systems. The information on the developed test rig can also be found in authors' other works [5, 22].

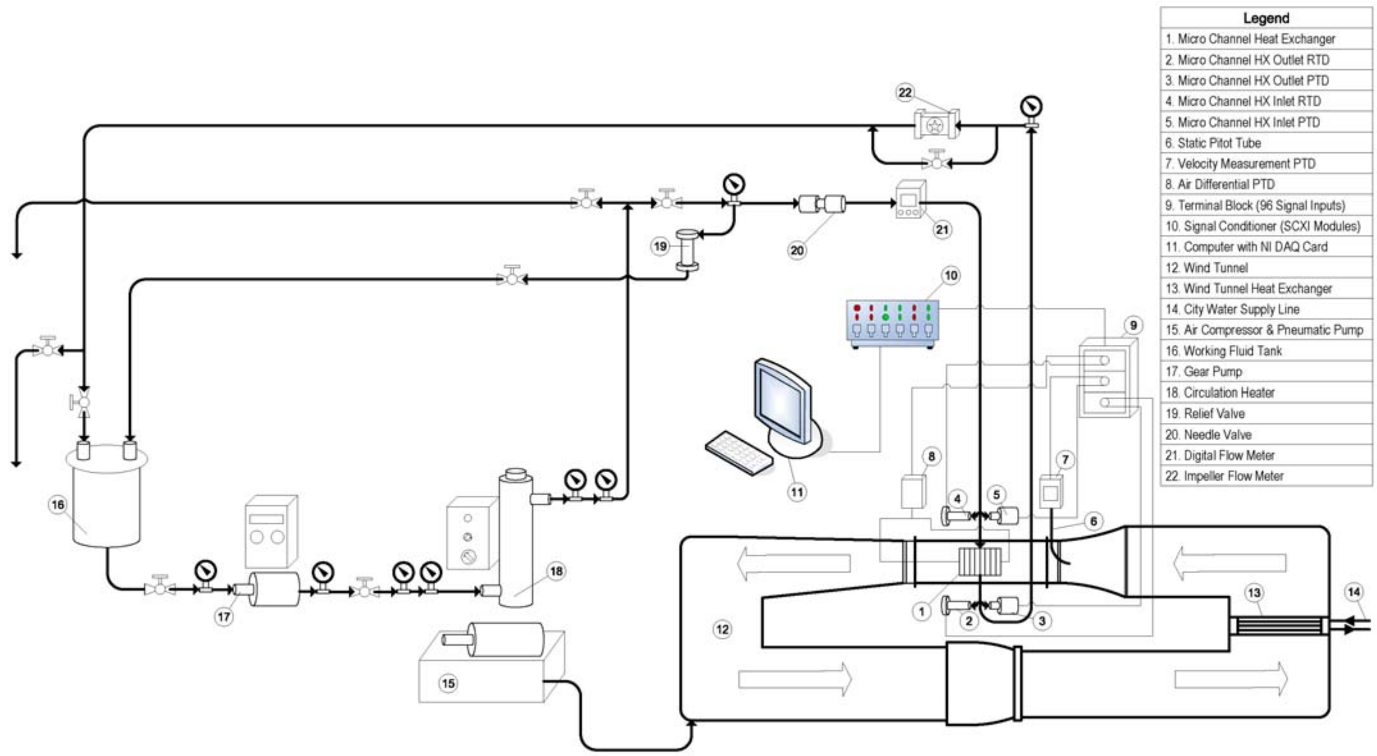

FIG. 1: SCHEMATIC OF THE DEVELOPED EXPERIMENTAL TEST FACILITY

Liquid handling system

As shown in Fig. 1, the liquid system consists of (16) fluid tank, (17) gear pump, (18) circulation heater, (19) pressure relief bypass valve and (20) micro-filter all are connected using Swagelok made stainless steel tubes, hoses and fittings. Arrangements have been kept to operate the system in either closed or open loop as necessary with the provisions for liquid drain out and system cleaning. A gear pump was chosen since it delivers a constant volume of liquid at a fairly steady flow rate regardless of the change in upstream pressure, which is the key for precise measurement data [20]. In addition, a needle valve is installed in the loop to provide further precision to the flow stability. The pump derives liquid from the source tank and pushes through the test specimen via the heating unit. The hot liquid transfers heat to the cold air stream flowing over the test slab and returns back to the source tank again (closed-loop) or exits to the atmosphere (open-loop).

Two inline digital flow meters are installed, primary one DFM (21) at the upstream and the secondary one as a backup IFM (22) at the downstream of the test section. In order to measure the flow pressure and temperature immediate before and after the test sample, two pressure transducers (PTD) one at inlet (5) and other at exit (3) and two ultra-precise RTD (Pt100) one at inlet (4) and other at exit (2) of the test specimen are installed. The specifications and accuracy data of the flow meter, PTD, and RTD are listed in Table 1 below.

TABLE 1. MEASURING SENSORS AND CALIBRATORS

Code	Descriptions of instruments	Capacity /Range	Accuracy
DFM (21)	Digital flow meters FV4000: Flow rate: 0.2 ~ 60 LPM $0 \le T \le 100$°C; $0 \le p \le 680$ kPa	0.2 ~ 2.2 LPM 0.4 ~ 5.3 LPM 4.5 ~ 60 LPM	$\dot{\forall}$:±0.5%FS T: ±1.1%FS p: ±1.1%FS
IFM	Impeller flow meter (22)	0.3 ~ 19 LPM 0.8 ~ 75 LPM	±1% FS ±1% FS
PTD	Pressure transducer, Liquid side (5) & (3)	0 ~ 103 kPa 0 ~ 345 kPa 0 ~ 689 kPa	±0.25% FS ±0.25% FS ±0.25% FS
RTD	Ultra precise RTD (4) & (2)	-100 ~ 400°C	±0.012°C
TC	Thermocouple Type-T	-200 ~ 350°C	±0.8°C
PTD	Pressure transducer differential, Air-side (7)	0 ~ 125 Pa 0 ~ 249 Pa 0 ~ 748 Pa	±0.25% FS ±0.25% FS ±0.25% F
HWA	Hotwire anemometer (VelociCalc)	0 ~ 30 m/s -18 ~ 93°C	±3% of rdg ±0.3°C
→ Airflow calibrator (FKT-3DP1A): 1) Absolute pressure transducer 2) Differential pressure transducer-1 3) Differential pressure transducer-2 4) Differential pressure transducer-3 5) Temperature sensor (TC reader) 6) Relative humidity (RH) sensor		1) 15 ~ 115 kPa 2) ±100 Pa 3) ±248.8 Pa 4) ±1.25 kPa 5) -200 ~ 177°C 6) 0 ~ 100% RH	1) ±0.5% FS 2) ±0.22% FS 3) ±0.22% FS 4) ±0.22% FS 5) ±0.5°C FS 6) ±2% FS
→ CL-770A Dry block calibrator (resolution ±0.01°C, stability in 5 min ±0.05°C):		-45°C (below ambient) ~ +140°C	±0.03°C

Air handling system

A closed-loop thermal environmental wind tunnel (12) serves the purpose of air handling system as portrayed in Fig. 1. The detailed descriptions and information are given by Khan et al. (2004, 2005) [23-24]. The tunnel with a contraction ratio of 6.25 is capable of producing the air velocities up to 30 m/s with no blockage and up to 25 m/s in presence of current test sample MCHX #4. An internal heat exchanger built-in to the wind tunnel (13) makes up the required hot or cold air by drawing pressurized hot or cold water from the attached mixing network (14). Two temperature measuring grids were designed and placed at the upstream and downstream of the wind tunnel test chamber to facilitate the precise measurement of airflow temperatures over the test slab. The inlet grid has 3 x 3 = 9 and the exit grid has 5 x 5 = 25 equally spaced type-T thermocouples. Reasonably well mixing of air molecules at the downstream was realized by measuring temperature using 25 equal grid points. The thermocouples are online calibrated and connected to the data acquisition (DAQ).

A Pitot static tube (6) in combination with an airside (7) differential pressure transducer (PTD) is mounted at the test chamber inlet to measure the air velocity. One FlowKinetics FKT series precision calibrator manometer is also connected for both calibration, monitoring and backup measurement of airflow and air velocity. The air distribution upstream to the test chamber was found almost flat and uniform and therefore the center point velocity measurement could represent the entire upstream cross-section with a multiplication factor of 0.90 [23-24]. In current study, a Pitot traverse survey on the wind tunnel based on *Log-Tchebycheff* point distributions [25] suggested this factor to be 0.875, which was used throughout the paper. A hot wire anemometer (HWA) is also installed for monitoring and backup measurements of air velocity. The specifications and of the instruments are given in Table 1.

Test chamber and test specimen

The test chamber in current study is 305 mm x 305 mm in vertical plane and 610 mm horizontal plane i.e. in the direction of airflow. It is made with 6.5 mm thick low thermal conductivity (0.19 W/m-°C) Plexiglas material. As seen in Fig. 2, the test sample MCHX #4 is mounted in the middle of the wind tunnel test chamber. The Plexiglas thick wall and its low thermal conductivity kept the test specimen in a sealed domain, which virtually did not take part in any heat transfer activity with the outside environment. Even so, additional insulation is provided to further ensure that there is no heat loss or gain from or to the test section. Now, only the heated segment of the test sample is exposed inside the test chamber for experimental forced convection heat transfer activity. A P012A-CF 12-inch Pitot static probe is placed at the center of the inlet cross-sectional plane to measure the airflow velocity.

The test specimen in current study (MCHX #4) is a finned serpentine 2-pass multi-port flat slab as shown in Fig. 3. This Aluminum alloy precision micro multi-port extrusion (MPE) sample was fabricated by Hydro Aluminum. The test specimens can withstand a working pressure of 15 MPa. As can be seen in Fig. 2, the test specimen is housed in the middle of the wind tunnel test chamber. Its inlet and exit header (manifold) tubes are connected to the liquid handling system via compression fittings. The information on the test sample is given in Table 2.

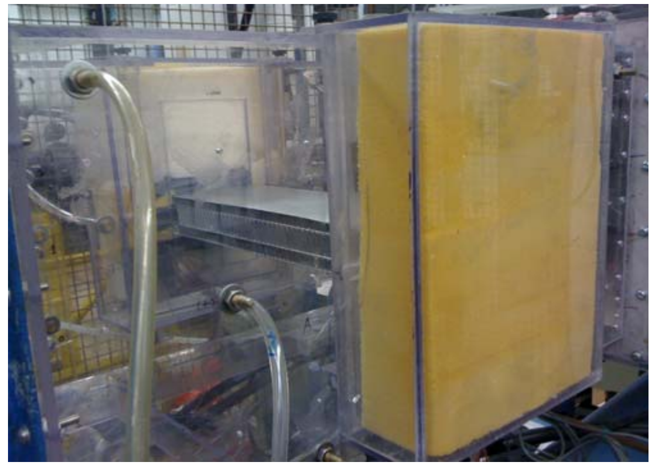

FIG. 2: TEST SPECIMEN INSIDE WIND TUNNEL TEST CHAMBER

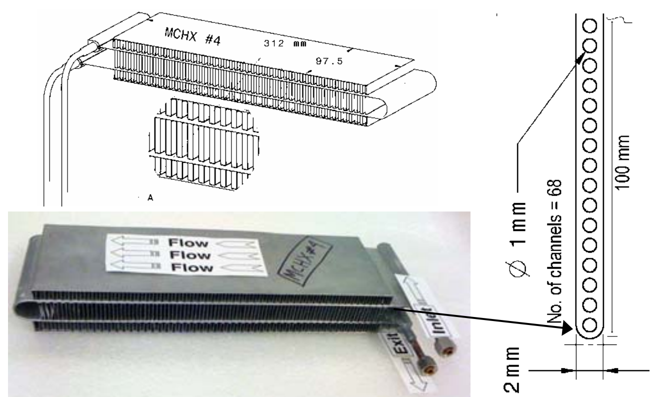

FIG. 3: TEST SPECIMEN USED IN CURRENT STUDY

TABLE 2. TEST SPECIMEN INFORMATION (UNITS, IN MM)

Parameters	Specimen ID: MCHX #4
Illustrating Figure No.	2
No. of channels in the slab, N_{ch}	68
Each channel diameter, D	1
Port-to-port distance, S	1.463
Slab width, W	100
Slab thickness, H	2
Serpentine internal diameter, d_{serp}	20
Fin type	Wavy
Fin density (fin/mm)	0.315
Fin height, H_{fin}	20-in/10-out
Fin thickness, t_{fin}	0.101

Data acquisition (DAQ) system

A 128-channel 16-bit NI data acquisition (DAQ) system has been integrated with the test bench in multiplex mode for automated monitoring and recording of experimental data. The DAQ system is identified in Fig. 1 by numbers (9), (10), and (11). The measuring instruments and sensors are connected to the DAQ except for two humidity sensors. These handheld digital humidity sensors are used to periodically monitor and record the humidity at test section inlet and exit.

Present configuration made the DAQ capable of handling 96 individual experimental parameters from 96 different locations through 96 separate channels. It can sample the data at a rate of 100 kHz. The faster the sampling rate the better the measurement accuracy. At the beginning, the DAQ channels were sampled at different rates to choose a suitable faster rate. Because of simultaneous measurements in total 96 separate channels in multiplex mode, 1 kHz sampling rate was chosen in order to avoid any possible data jam or system interruptions.

Calibration of instruments and sensors

The manufacturer had supplied the glycol-water mixture calibration data for the digital flow meters. They were verified with balance-weigh method and the output voltages were found fairly linear. The airside and liquid side pressure transducers are also supplied with calibration data using NIST traceable instrumentation and standards. The installed Pitot static probe and associated differential pressure sensor was offline calibrated along with the wind tunnel using the FlowKinetics FKT series precision calibrator manometer. After calibration, the pressure transducer was tested by running the system at various air velocities and their outputs were recorded and verified. The adopted calibration was found consistent with the manufacturer supplied calibration data.

The temperature sensors, the RTDs and the thermocouples were calibrated at 5°C intervals directly online at the DAQ system using a precise and highly stable Omega CL-770A dry block calibrator. After adopting the calibrations, the reading of the probes were verified by running the test rig with some given temperatures. It was seen that all the thermocouples read and measured within ±0.04°C and the RTDs within ±0.008°C.

Experimental procedures

At the beginning several trial experiments were conducted at various flow rates to observe and obtain the overall system stabilization time and instrumental responses. Each of the experiments was carried out at steady-state condition, which was considered reached when the fluctuations of the flow rate and temperature of the fluid were no more than 2% for longer time period. To reach the steady-state condition, on an average, the liquid side took around 1 hour and airside took around 30 minutes. Hot 50% ethylene glycol-water solution was pumped through the test sample in the Reynolds number range between 400 and 1800 and the cold wind tunnel air was blown over the test slab with a constant velocity of 16.70±0.20 m/s. The hot glycol-water inlet temperature i.e. inlet to the test specimen was maintained at 76.0±0.4°C and the bulk temperature of the cold airflow was kept constant at 9.0±0.2°C.

The inlet temperature of liquid was maintained using heater controller and the airside bulk temperature was realized by manipulating the cold water flow rate through the heat exchanger built-in with the wind tunnel. The liquid side flow rates were varied and maintained with the aid variable speed gear pump and a needle valve. At each liquid flow rate step, required time was allowed to achieve the steady-state condition before any data collection was begun.

At each flow rate, thousands of samples were collected for each parameter and their mean and standard deviations were documented. A single data set in current study is the time averaged mean data set (TAMDS) of around 10000 to 15000 steady state samples for each measured parameter. The data acquiring method can be represented by Eq. (1).

$$\overline{TAMDS} = \frac{1}{k}\sum_{m=1}^{k}\left[\frac{1}{n}\sum_{\mathrm{n}=1}^{n} TAMDS_{\mathrm{n}}\right] \tag{1}$$

where n = 10000 ~ 15000, and k = 2 ~ 4 repetitions.

DATA REDUCTION AND UNCERTAINTY ANALYSIS

The focus of current study was on liquid side i.e. the 50% ethylene glycol-water mixture flow in multi-port serpentine meso-channel slab. Assumptions were made that the liquid is incompressible Newtonian fluid and its properties are independent of pressure but the functions of temperature only. The liquid was assumed to be uniformly distributed through all the channels in the test slab, which was reasonable consideration because the distributing manifold was about 10 times the diameter size of a single channel of the test slab. The primary independent parameters i.e. the mass flow rate ($\dot{m}_{\mathrm{g}}$), temperatures (T_{g}), and pressures (p_{g}) of the liquid and the velocity (V_{a}), temperatures (T_{a}), and pressures (p_{a}) of airflow were directly measured for 20 different operating conditions. The thermophysical properties of the liquid for each data point were evaluated at the bulk temperatures derived from the ASHRAE Handbook of fundamentals 2001 [26].

The Reynolds number of the liquid (Re_{g}) flow in a single channel is then calculated using mass conservation principle $\dot{m}_{\mathrm{g}} = (\rho AV)_g$ and is given as follows.

$$\mathrm{Re}_{\mathrm{g}} = \left(\frac{\rho VD}{\mu}\right)_g = \frac{4\dot{m}_{\mathrm{g}}}{\pi\mu_{\mathrm{g}} D N_{\mathrm{ch}}} \tag{2}$$

The forced convection heat transfers between liquid and air were estimated for respective side of the fluids as follows.

$$q_{\mathrm{g}} = \dot{m}_{\mathrm{g}} c_{\mathrm{p,g}} (T_{\mathrm{g,i}} - T_{\mathrm{g,o}}) = C_{\mathrm{g}} \Delta T_{\mathrm{g}} \tag{3}$$

and

$$q_a = \dot{m}_a c_{p,a}(T_{a,o} - T_{a,i}) = C_a \Delta T_a \,. \qquad (4)$$

Ideally the above heat rates should be the same since the heat released by the liquid is taken away by the air i.e. $q_g \approx q_a$. However, practically this is rarely the case because of the existence of errors in system response, experiments, heat leakage etc. The percentage difference between the heat lost by liquid q_g and that gained by air q_a is therefore defined as the heat balance (HB) in current study as expressed by Eq. 5.

$$HB_g = \frac{q_g - q_a}{q_g} * 100 \,. \qquad (5)$$

As will be shown next in results and discussions section, the average HB was also verified with ASME PTC 30-1991 recommended acceptable limit [27] for an air-cooled heat exchanger using the following expression.

$$HB_{avg} = \left| \frac{q_g - q_a}{q_{avg}} \right| * 100, \text{ where, } q_{avg} = \frac{(q_g + q_a)}{2} \qquad (6)$$

Because of using ultra precise RTD for liquid side temperature measurements, using the liquid side heat rate q_g in subsequent calculations could be more reliable choice. The overall thermal resistance, R_{ov} was computed from q_g to be,

$$R_{ov} = R_g + R_{wall} + R_a = \frac{1}{UA} = \frac{\Delta T_{lm} F}{q_g} \,. \qquad (7)$$

The crossflow correction factor F was obtained from Bowman et al. (1940) [28]. The P and R temperature loadings in present experiments were such that for all the data sets the F varied between 0.994 and 0.998. The log-mean temperature difference (LMTD) was defined by Eq. (8) as follows [28]:

$$\Delta T_{lm} = \frac{\Delta T_1 - \Delta T_2}{\ln\left(\Delta T_1 / \Delta T_2\right)}, \text{ where } \begin{cases} \Delta T_1 = T_{g,i} - \Delta T_{a,o} \\ \Delta T_2 = T_{g,o} - \Delta T_{a,i} \end{cases}. \qquad (8)$$

For a heat transfer route from bulk liquid side to the bulk airs flow, the overall thermal resistance $R_{ov} = 1/UA$ for current test specimen can be written in the following form,

$$R_{ov} = \frac{1}{UA} = R_g + R_{wall} + R_a = \frac{1}{h_g A_{s,g}} + R_{wall} + \frac{1}{\eta_o h_a A_{tot,s,a}} \quad (9)$$

The thickness of the test sample wall is very small and the thermal conductivity of the wall material is high. Therefore for simplicity in analyses the wall thermal resistance was dropped from Eq. (9) i.e. it was set as $R_{wall} \approx 0$.

To characterize an array of fins at airside, the overall surface efficiency or temperature effectiveness is given by [29]

$$\eta_o = 1 - \frac{A_{fin}}{A_{tot,s,a}}(1 - \eta_{fin}) \qquad (10)$$

The fin efficiency for wavy fins of uniform cross-section similar to current slab is described by Shah and Sekulic (2003) [29], which were adopted in MCHX #4 test sample as follows.

$$\eta_{fin} = \frac{\tanh(ML)}{ML}, \text{ where } \begin{cases} M \approx \sqrt{\dfrac{2h_a}{k_{fin} t_{fin}}} \\ L = \dfrac{H_{fin}}{2} - t_{fin} \end{cases} \qquad (11)$$

The fin efficiency η_{fin} varied between 0.905 and 0.912 in this study and the overall surface efficiency η_o between 0.918 and 0.924, which are seen to stay almost constant for all the data sets at 0.908±0.0035 and 0.920±0.0031 respectively.

The glycol-water side and the airside thermal resistances $R_g = 1/h_g A_{s,g}$ and $R_a = 1/\eta_o h_a A_{tot,s,a}$ and hence the individual heat transfer coefficients h_g and h_a were separated from Eq. (9) using modified Wilson Plot Technique as described next.

Information on surface temperature T_s is necessary to calculate the individual fluid side heat transfer coefficient from the measured heat rate. Measuring T_s for a finned surface like the one used in current study is very difficult and there the Wilson Plot Technique plays role without this information. An attempt was made to measure the T_s of MCHX #4 immediate before and after the test section and around the serpentine using 48 thermocouples placed on un-finned exposed surface. This approach was taken to compare the results obtained from the Wilson Plot Technique with this measurement. Constant surface temperature boundary condition was assumed to be closer to the current experimental situations.

The mean of the measured T_s for each data set was used to separately calculate the liquid side and airside heat transfer coefficients h_g and h_a using Newton's law of cooling.

$$h_g = \frac{q_g}{A_{s,g}(T_g - T_s)} \qquad (12)$$

and

$$h_a = \frac{q_g}{\eta_o A_{tot,s,a}(T_s - T_a)} \qquad (13)$$

The heat exchanger effectiveness of the test slab was realized from the following relation,

$$\varepsilon = \frac{q_g}{q_{max}} = \frac{q_g}{C_{min}(T_{g,i} - T_{a,i})} \quad (14)$$

and the number of transfer unit (NTU) for the current test slab was determined from the following relationship,

$$NTU = UA/C_{min} \quad (15)$$

The calculation of liquid side Nusselt number Nu_g from the measured heat rate q_g and measured surface temperature T_s was based on Eq. (16) below.

$$Nu_g = \frac{h_g D}{k_g} \quad (16)$$

In a developing laminar pipe flow the Nu_g generally depends on Re_g and Prandtl number Pr_g. Therefore, for working with Wilson Plot Technique the Nu_g was defined in the form,

$$Nu_g = \frac{h_g D}{k_g} = C_1 Re_g^a Pr_g^{1/3}. \quad (17)$$

Wilson Plot Technique

This method was originally devised by Wilson in 1915 for separating the individual thermal resistances from a two-fluid single-phase heat exchanger without the information of surface temperature [30]. By assuming a tube side Re exponent of 0.82, the two unknowns i.e. the shell side resistance and the tube side Re coefficient were determined from a regression analysis. Over the decades, modifications and improvements have been proposed by different authors to apply this method on a variety of heat exchangers for the situation with more than two unknowns. In other words, when the Re coefficients and exponents are unknown for both the fluids. Briggs and Young (1969) proposed a modification to the original method for determining three unknowns rather than two through two-step successive linear regression analyses of a non-linear equation, which is so called the "modified Wilson Plot Technique" [31].

On finding some convergence problem for some data sets in using Briggs and Young proposed modification, Khartabil and Christensen (1992) presented an improved non-linear regression scheme, which according to the authors guarantee the convergence if a solution exists [32].

In order to apply the Wilson Plot Technique, some restrictions in conducting experiments apply. They are: (a) all the data sets must be taken in a single flow regime, (b) the flow rates of the fluid of interest be varied and the flow rate of other fluid must be kept constant for the entire data sets, and (c) the bulk temperature of the constant flow fluid also be kept constant to allow the thermal resistance of that fluid to remain same. In current study the liquid side was the focus and therefore the experiments were accordingly carried out by maintaining the airside conditions fairly constant.

Uncertainty analysis and error estimation

The accuracy information of the instruments and sensors is based on manufacturer's data and the accompanying documentation. The accuracy listed in Table 2 is the overall instrument error, which is estimated from the root sum square (RSS) of all known errors using Eq. (18). This includes all errors like resolution, linearity, repeatability, sensitivity, hysteresis, scale effect (FSO), zero offset, precision, various drifts, reproducibility etc.

$$I_{RSS} = \sqrt{I_1^2 + I_2^2 + \ldots\ldots\ldots + I_n^2} \quad (18)$$

where I is the instruments' known error(s) 1, 2, …..n and the I_{RSS} is the overall instrument error.

The experimental uncertainty analysis can be carried out in light of the ASME Journal of Heat Transfer Editorial (1993) and ASME Journal of Fluids Engineering Editorial (1991) [33-34]. Other available resources can also be consulted [3, 35]. Errors from the on the measured primary parameters propagate into the secondary variables depending on their relationships. If A is a secondary parameter, which depends on other primary measured parameters like A_1, A_2, A_3, … then the errors from measured primary parameters propagate into the secondary parameter A according to the relationship between A and A_1, A_2, A_3, ….. The absolute uncertainty U of A is then calculated using root sum square (RSS) method as given by Eq. (19).

$$U_A = \sqrt{\left(\frac{\partial A}{\partial A_1} U_{A_1}\right)^2 + \left(\frac{\partial A}{\partial A_2} U_{A_2}\right)^2 + \ldots\ldots} \quad (19)$$

The partial derivatives $\partial A/\partial A_1, \partial A/\partial A_2, \partial A/\partial A_3$ ... of the secondary or dependent parameters are derived from their relationship with the primary or independent parameters.

The individual uncertainties of the independent parameters $U_{A_1}, U_{A_2}, U_{A_3}, \ldots$ are estimated from the bias and precision of both the experiments and instruments (I_{RSS} from Eq. 18) errors. The relative uncertainty is generally obtained by dividing the absolute uncertainty by the mean value as shown in Eq. (20) below.

$$\frac{U_A}{\bar{A}} = \sqrt{\frac{\left(\frac{\partial A}{\partial A_1} U_{A_1}\right)^2 + \left(\frac{\partial M}{\partial M_2} U_{A_2}\right)^2 + \ldots..}{\left[f(A_1, A_2, \ldots\ldots.)\right]^2}} \quad (20)$$

The estimated mean uncertainties for the liquid side key parameters in current study are tabulated in Table 3.

TABLE 3. MEAN UNCERTAINTIES

Liquid-side parameters	Uncertainty
Measured pressure drop (Δp_g), Pa	±6.0 %
Mass flow rate ($\dot{m}_g$), kg/s	±4.5 %
Reynolds number (Re_g)	±6.5 %
Nusselt number (Nu_g)	±12.5 %

RESULTS AND DISCUSSIONS

Pressure drop (Δp_g)

The liquid side pressure drop, Δp_{total} was measured before and after the inlet and exit manifolds of the test slab, which included core and other pressure losses. For data comparison purpose, the pressure drop along the core of the test slab was isolated from Δp_{total} by following the empirical approximations used by Jokar et al. (2010) and Kasagi et al. (2003) [17, 36]. The theoretical Δp for fully developed conventional laminar pipe flow is also compared, which was taken from Poiseuille equation in the following form for current conditions.

$$\Delta p_{\mathrm{Po,theory}} = \frac{128\mu_g L_{\mathrm{hyd}}}{\pi D^4}\dot{V}_g = \frac{128\dot{m}_g \mu_g L_{\mathrm{hyd}}}{\pi \rho_g D^4 N_{\mathrm{ch}}} \quad (21)$$

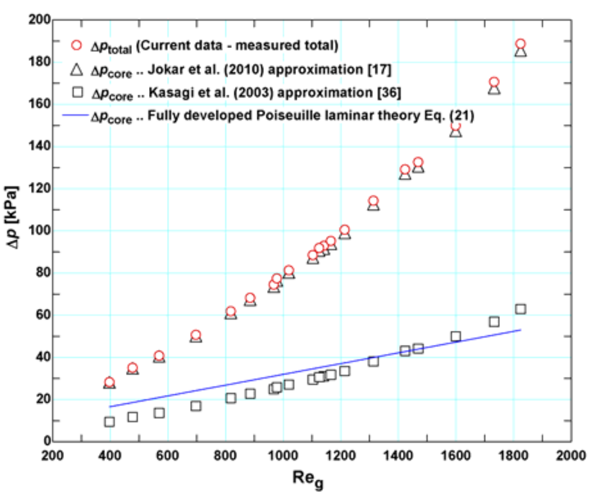

FIG. 4: VARIATION OF PRESSURE DROP WITH REYNOLDS NUMBER (GLYCOL-WATER MIXTURE)

The Δp_{total} and Δp_{core} are plotted against Re_g in Fig. 4. All the Δp increased generally non-linearly with the increase of Re except for the Poiseuille Δp, which increased linearly. The non-linear variations may be due to the flow development effects since the Δp is always higher around entrance regime. While Kasagi et al. approximation showed closeness to the Poiseuille Δp, it however estimated lower Δp for the entire Re_g range. Jokar et al. approximation on the other overestimated current core Δp. Their channel had some bumps; as a result the core Δp might have been dominated by frictional Δp and that their approximation possibly only valid in their test situations. Removals of all the possible losses from current measured Δp could represent the comparisons better, which however were not performed within the scope of current study.

Heat transfer rates (q_g and q_a)

Determined from Eq. (3), the glycol-water mixture heat transfer rate q_g is plotted in Fig. 5 against Re_g. The q_g increased with the increase of Re_g, which is expected. The variation followed a power-law relationship better with R^2 value of 0.964. Few scatters in data as seen in higher Re_g may have generated from little flow and temperature fluctuations. About 4 kW of heat transfer rate could be achieved from the test slab with an LMTD of 61°C within current test conditions.

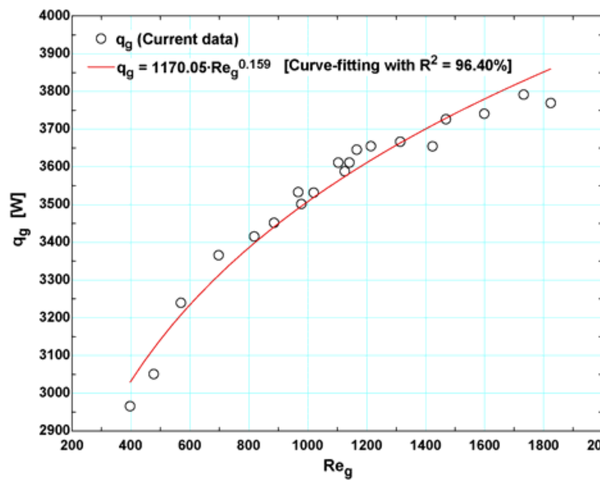

FIG. 5: VARIATION OF HEAT TRANSFER RATE WITH REYNOLDS NUMBER (GLYCOL-WATER MIXTURE)

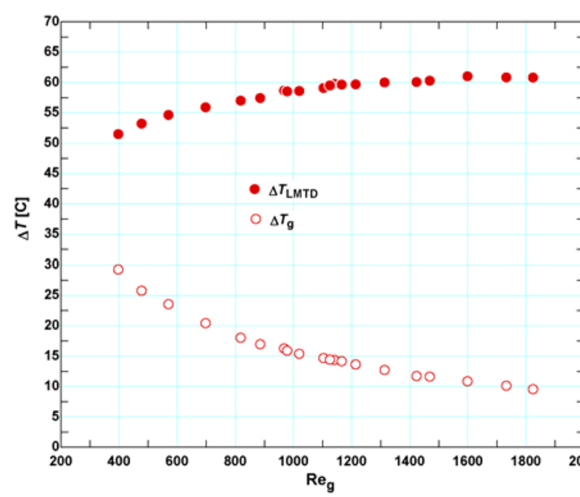

FIG. 6: VARIATION OF TEMPERATURE DIFFENENTIALS WITH REYNOLDS NUMBER (GLYCOL-WATER MIXTURE)

The liquid side ΔT_g and the overall ΔT_{lm} calculated from Eq. (8) are portrayed in Fig. 6 with Re_g. The ΔT_g decreased in a power manner with negative exponent with the increase of mass flow rate and hence the Re_g. The ΔT_{lm} increased with the increase of Re_g in power-law pattern with positive exponent.

The airside heat rate q_a estimated from Eq. (4) is displayed in Fig. 7 against q_g in order to compare the variation. The data followed a linear variation with some scatters within ±2.5%.

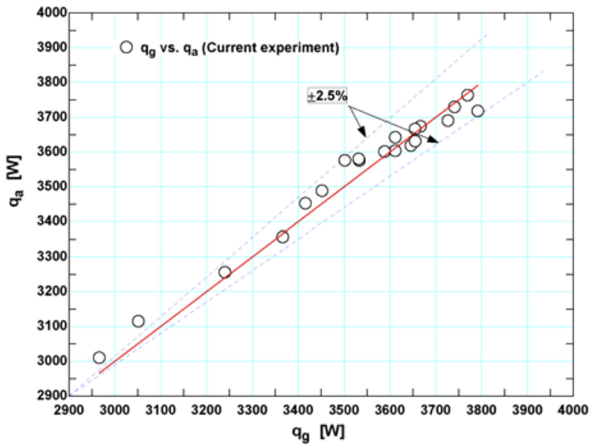

FIG. 7: DEVIATIONS OF AIRSIDE HEAT TRANSFER RATE FROM THAT OF GLYCOL-WATER SIDE

As defined by Eqs. (5) & (6), the heat balance HB between liquid side and airside are performed to realize the deviations of q_a from that of q_g and q_{avg}. The HB results are presented in Fig. 8 with respect to Re_g. The deviations of q_a were observed to be from -2.13% to +1.93% and -2.11% to +1.95% from q_g and q_{avg} respectively. Both data are overlapped because the deviations are less and similar. This good enough HB shows the integrity of the developed test facility.

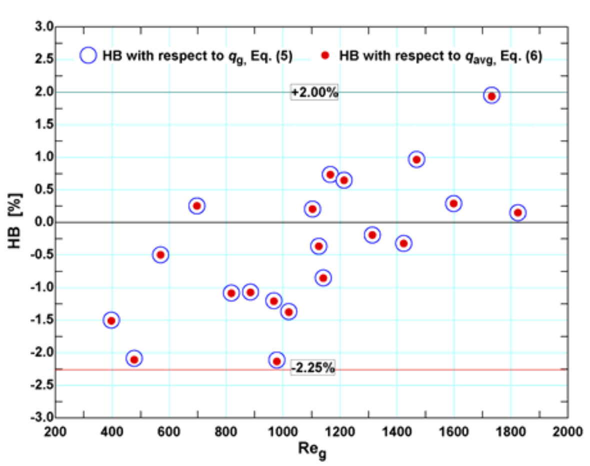

FIG. 8: HEAT BALANCE BETWEEN AIRSIDE AND GLYCOL-WATER SIDE WITH REYNOLDS NUMBER

The ASME PTC 30-1991 recommends an acceptable limit of ±15% for which any of the heat rates i.e. q_g, q_{avg}, or q_a can be used for heat transfer calculations. As mentioned before, the liquid side heat rate q_g was taken in current study for all the calculations.

The NTU and Effectiveness (ε) of the test slab

By viewing the test sample in present study as a small piece of heat exchanger, its effectiveness ε and NTU can be determined from Eqs. (14) and (15) using measured data. The ε and NTU are graphically presented in Fig. 9 with respect to Re_g. Both the ε and NTU monotonically decreased with the increase of Re_g. The ε decreased from 0.43 to 0.14 and the NTU from 0.57 to 0.16. For a given Re_g, Fig. 9 can provide values of both ε and NTU.

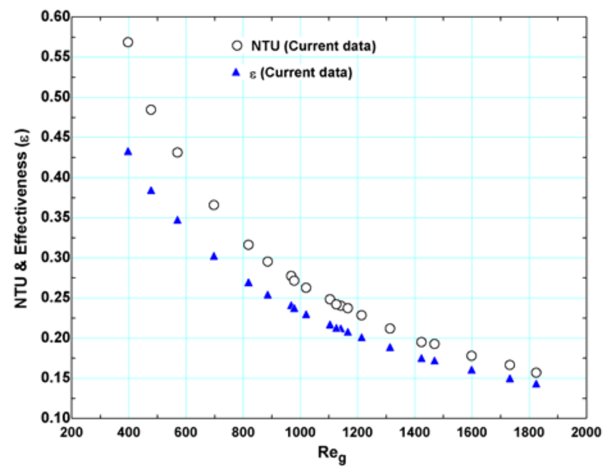

FIG. 9: VARIATIONS OF NTU AND EFFECTIVENESS WITH GLYCOL-WATER SIDE REYNOLDS NUMBER

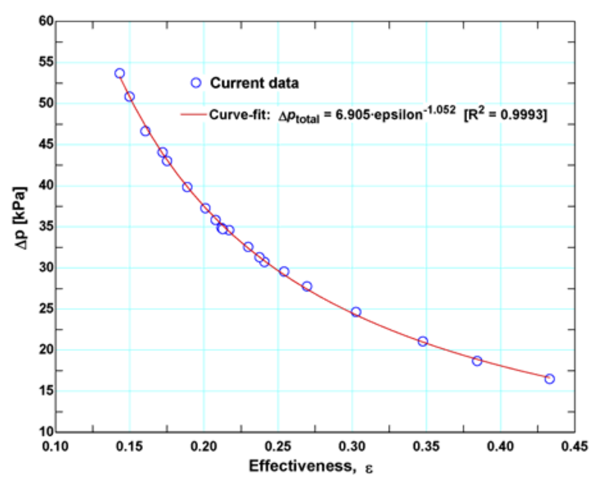

FIG. 10: VARIATIONS OF GLYCOL-WATER SIDE Δp WITH TEST SLAB EFFECTIVENESS

The heat transfer rate q_g and the pressure drop Δp both are plotted against ε in Fig. 11. Both the q_g and Δp decreased when ε increased. The q_g decreases linearly and Δp decreases in power-law manner. At higher ε both the q_g and Δp are lower and at lower ε they both are higher. This kind of parametric plotting will help optimize an operating point for a particular chosen duty. The trends of current results in Fig. 11 showed excellent qualitative agreement with Kang and Tseng [37].

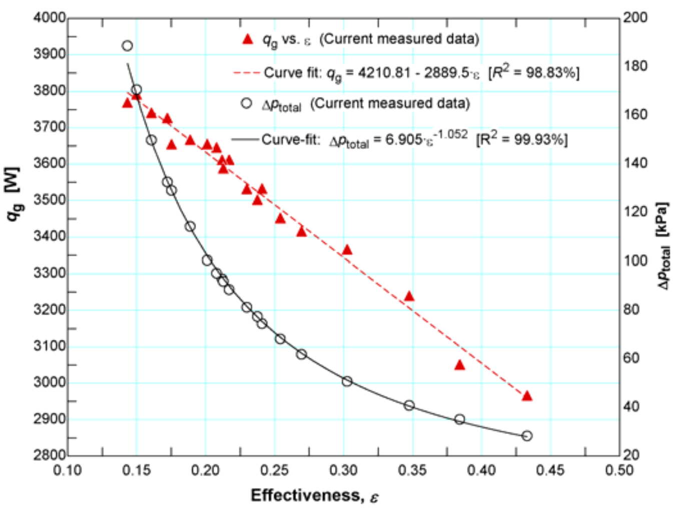

FIG. 11: VARIATIONS OF GLYCOL-WATER SIDE q_g AND Δp_{total} WITH RESPECT TO TEST SLAB EFFECTIVENESS

Overall thermal resistance (R_{ov} = 1/UA)

The overall thermal resistance R_{ov} based on experimentally measured parameters was calculated from Eq. (7). The same R_{ov} was also predicted using Khartabil and Christensen (1984) improved scheme [32] based on Briggs and Young (1964) proposed [31] modified Wilson Plot Technique. Both the resistances are plotted in Fig. 12 against Re_g. The R_{ov} asymptotically decreased with the increase of Re_g. The R_{ov} predicted from Wilson plot method was well bounded by the scatters in experimentally measured R_{ov} data as can be seen in Fig. 12. The maximum deviation between the measured and the predicted results was no more than ±1.50%.

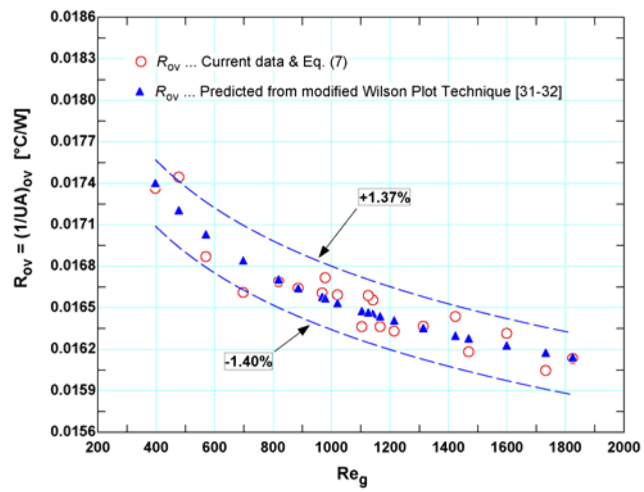

FIG. 12: VARIATIONS OF OVERALL THERMAL RESISTANCE R_{ov} WITH GLYCOL-WATER SIDE Re_g

Nusselt number (Nu_g) at glycol-water side

The Nu_g was deduced from Eqs. (12) & (16) based on the mean T_s measured at 48 different locations on the test slab exposed surface. Two other Nu_g were predicted separately one from Briggs and Young (1964) proposed modified Wilson Plot Technique [31] and another from Khartabil and Christensen (1984) improved scheme [32]. All the Nu_g are plotted against Re_g in Fig. 13. Expectedly Nu_g increased with the increase of Re_g and the curve followed power-law relationships. Predictions from Briggs & Young two successive regression analyses differed from Khartabil & Christensen non-linear regression scheme, i.e. underestimated the Nu_g values.

The experimental Nu_g values are always higher than the Briggs & Young method. The experimental Nu_g values are however higher than Khartabil & Christensen scheme only in the range $400 \le Re_g \le 1300$, beyond which they overlap each other. There are scatters in experimental Nu_g data more in the range $400 \le Re_g \le 1300$. This can be explained that the T_s were more stable at higher Re than lower. Some of the T_s were also measured around the bend at serpentine; there due to flow reversal action the T_s might have experienced different profiles at lower Re than higher. As seen from the error bars in Fig. 13, the experimental Nu_g data cover the Khartabil & Christensen prediction very well than the Briggs & Young prediction.

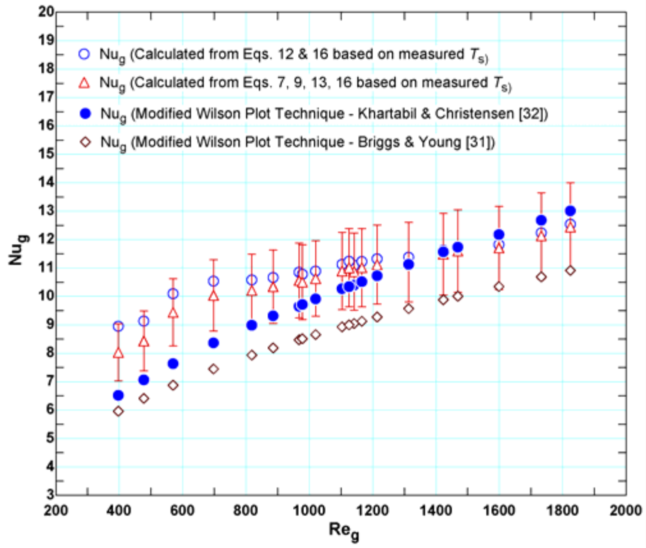

FIG. 13: VARIATIONS OF NUSSELT NUMBER WITH REYNOLDS NUMBER (GLYCOL-WATER MIXTURE)

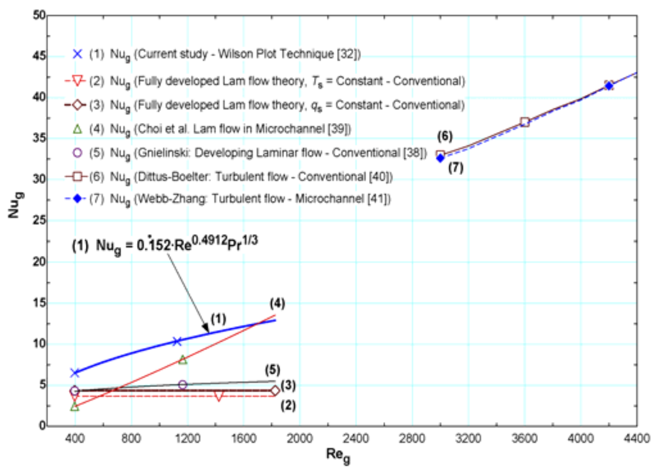

FIG. 14: NUSSELT NUMBER VS. REYNOLDS NUMBER COMPARISON WITH AVAILABLE CORRELATIONS

From a curve-fit, heat transfer correlation for developing flow was obtained in the form of $Nu_g = 0.152\,Re_g^{0.4912}\,Pr_g^{1/3}$ for the range $400 \le Re_g \le 1800$ tested in current study. In Fig. 14, the current Nu_g are compared with available correlations. None of the conventional or microchannel correlations could compare current Nu_g data well. Current results are higher than both T ($Nu_T = 3.66$) and H ($Nu_H = 4.36$) boundary fully developed conventional values and also higher than the conventional thermally developing laminar flow correlation proposed by Gnielski (1976) [38].

Choi et al. (1991) [39] proposed correlation for laminar microchannel flow crossed current Nu_g values for Reg > 1600. Current Nu_g values were however lower than the Dittus & Boelter (1930) [40] conventional turbulent correlation and Webb & Zhang (1998) [41] microchannel turbulent correlation, which can be seen from for the less steep slope of present Nu-Re curve.

Several factors may be responsible for this higher Nu_g values in present study such as the presence of serpentine, internal narrowness at the entrance and exit connectivity due to manufacturing imperfections, inner channel shrinking due to bending around serpentine, flow developing nature different from conventional case of $L_{th} = 0.05RePrD$ etc. However, the authors believe that the presence of serpentine being the major reason.

At the lowest flow rate the fully developed status was attained at 70% of the slab flow length before approaching the serpentine provided that the conventional developing length relationship applies. For any increase in flow rate the developing length was further extended. Therefore before traveling to the point of fully developed length the flow was reversed at the serpentine and a new entrance was formed as a result none of the flow was thermally developed in current experiments.

Understandable is that the flow reversal around a serpentine promotes heat transfer as well as pressure drop. Whether this effect is similar or different from the conventional entrance effect is not however clearly established. Further investigation is necessary using some narrow channel applied geometry like the one used in current study.

Conclusions

The multi-port finned or un-finned serpentine flat slabs as the core elements and the ethylene glycol-water mixture as the heat transfer fluid are frequently encountered in practical heat exchangers. Research on these applied geometries and on this fluid using narrow channel is rare in the open literature. In present study, experiments have been conducted on 50% ethylene glycol-water solution flow in a multi-port finned serpentine meso channel (1 mm) flat slab in liquid-to-air crossflow orientation. The liquid attained the developing laminar flow in the Reynolds number range between 400 and 1800. The objectives of the study were to investigate the heat transfer characteristics of the test fluid and performance of the test slab and to gather experimental data. Only the liquid side results are presented here.

The uncorrected Δp ranged from 30 to 190 kPa and non-linearly increased with Re_g. About 4 kW of heat rate could be achieved from the test slab with the LMTD of 61°C in the test conditions considered. The q_g increased with Re_g in power-law manner and decreased with ε linearly. NTU and ε both decreased with Re_g as well as with Δp. The NTU and ε values were found to be 0.16 to 0.57 and 0.14 to 0.43 respectively.

The Nu_g determined experimentally and predicted from modified Wilson Plot Technique both are comparable. As expected the Nu_g increased with Re_g in power law relationship and the mean value was higher than the values of conventional laminar developing flow correlations. This higher trend might have been attributed to the presence of serpentine and to the effects of developing flow. It is understandable that the flow reversal around a serpentine promotes heat transfer as well as the pressure drop. However, this effect is similar to or different from the entrance effect of narrow channels is not clearly known. Detailed investigation is necessary using some applied geometry like the one used in current study.

For the studied geometry in the range $400 \leq Re_g \leq 1800$, a heat transfer correlation for developing flow is obtained in the form of $Nu_g = 0.152\, Re_g^{0.4912}\, Pr_g^{1/3}$, which can be useful in the design and may serve as a roadmap in this promising area.

NOMENCLATURE

$\dot{m}_g$	Ethylene glycol-water total mass flow rate [kg/s]
$\dot{\forall}$	Liquid volume flow rate [m^3/s]
$\dot{m}$	Mass flow rate [kg/s]
A	Area [m^2]
c_p	Specific heat [J/kg.C]
D	Diameter of a single channel in test slab [m]
DAQ	Data acquisition system
DFM	Digital flow meter
D_h	Hydraulic diameter (= $4A/P$) [m]
d_{serp}	Serpentine diameter [m]
F	Correction factor for crossflow [-]
f	Represents function sign in equation (20)
H	Test slab thickness [m]
HB	Heat balance [%]
H_{fin}	Fin height [m]
HWA	Hotwire anemometer
IFM	Impeller flow meter
I_{RSS}	Instruments' RSS error
L_{hyd}	Hydrodynamic length of the test slab [m]
LMTD	Log-mean temperature difference [°C]
LPM	Liter per minute
MCHX	Microchannel heat exchanger
MPE	Multi-port extruded
N_{ch}	Number of channels in the test slab (= 68)
NTU	Number of transfer unit
Nu	Nusselt number
p	Pressure [Pa]
PTD	Pressure transducer
q	Heat transfer rate [W]
R	Thermal resistance [°C/W]
Re	Reynolds number
RSS	Root sum square
RTD	Resistance temperature detector
T	Temperature [°C]
TAMD	Time averaged mean data set
t_{fin}	Fin thickness [m]
U	Overall coefficient [W/m^2.C]; Uncertainty
V	Mean velocity of flowing fluid [m/s]
W	Test slab width [m]

Greek letters

μ	Dynamic viscosity of fluid [kg/m-s or N-s/m^2]
ρ	Density of flowing fluid [kg/m^3]
ε	Effectiveness of the test slab [-]
Δp	Pressure difference or pressure drop [Pa]
Δp_{core}	Only the pressure drop inside microchannel slab i.e. excluding all other inlet & exit losses in the route
ΔT_{lm}	Log-mean temperature difference [°C]
η_o	Overall surface efficiency [%]
η_{fin}	Overall fin efficiency [%]

Subscripts

a	Air
avg	Average
b	Bulk
ch	Channel
g	Ethylene glycol-water mixture
h	Hydraulic
i	Inlet or entrance
lm	Log-mean
max	Maximum
min	Minimum
o	Outlet or exit
ov	Overall
s	Surface
tot	Total
wall	Test slab wall

ACKNOWLEDGMENTS

The authors gratefully acknowledge the financial supports from the Natural Sciences and Engineering Research Council of Canada (NSERC) Canada Foundation for Innovation (CFI) for the current study. The authors recognize technical supports provided by the University of Windsor technologists Mr. Andrew Jenner and Mr. Patrick Seguin during the construction phase of the test facility. The authors are thankful to Mr. Faisal Siddiqui, a MASc student at University of Windsor for his help in drawing the schematic of the experimental facility.

REFERENCES

1. Steinke, M.E. and Kandlikar, S.G. "Single-phase liquid friction factors in microchannels." *International Journal of Thermal Sciences* 45, (2006) 1073-1083.
2. Morini, G.L., "Single-phase convective heat transfer in microchannels: a review of experimental results." *International Journal of Thermal Sciences* 43, no. 7 (2004) 631-651.

3. Kandlikar S.G., Garimella, S., Li D., Colin, S., and King, M.R. "Heat Transfer and Fluid Flow in Minichannels and Microchannels". Elsevier Ltd.: Oxford (2006).

4. Steinke, M.E., and Kandlikar, S.G. "Review of single-phase heat transfer enhancement techniques for application in microchannels, minichannels and microdevices." *International Journal of Heat and Technology* 22, no. 2 (2004) 3-11.

5. Khan, M.G., Siddiqui, F.A., Mosa, M.A.M. and Fartaj, A. "Experimental comparative study on heat transfer performances of circular, elliptical, and microchannel heat exchangers." *Proceedings of the Canadian Society for Mechanical Engineering Forum 2010 (CSME FORUM 2010)* Paper #162 (submitted), June 7-9, 2010, Victoria, BC, Canada

6. Hasan, M.I., Rageb, A.A., Yaghoubi, M., and Homayoni, H. "Influence of channel geometry on the performance of a counter flow microchannel heat exchanger." *International Journal of Thermal Sciences* 48, (2009) 1607-1618.

7. Garimella, S., Dowling, W.J., Veen, M.V.D., and Killion, J.D. "The effect of simultaneously developing flow on heat transfer in rectangular tubes." *Heat Transfer Engineering* 22, no. 6 (2001) 12-25.

8. Agostini, B., Watel, B., Bontemps, A., and Thonon, B. "Friction factor and heat transfer coefficient of R134a liquid flow in mini-channels." *Applied Thermal Engineering* 22, (2002) 1821-1834.

9. Agostini, B., Watel, B., Bontemps, A., and Thonon, B. "Liquid flow friction factor and heat transfer coefficient in small channels: an experimental investigation." *Experimental Thermal and Fluid Science* 28, (2004) 97-103.

10. Agostini, B., Bontemps, A., and Thonon, B. "Effects of geometrical and thermophysical parameters on heat transfer measurements in small-diameter channels." *Heat Transfer Engineering* 27, no. 1 (2006) 14-24.

11. Stignor, C.H., Sunden, B., and Fahlen, P. "An experimental study of liquid-phase heat transfer in multiport minichannel tubes." *Heat Transfer Engineering* 30, no. 12 (2009) 941-951.

12. Cheng, L. and Cees W.M.-V-D-G. "Experimental study of heat transfer and pressure drop characteristics of air/water and air-steam/water heat exchange in a polymer compact heat exchanger." *Heat Transfer Engineering* 26, no. 2 (2005) 18-27.

13. Kang, S.-W. and Tseng, S.-C. "Analysis of effectiveness and pressure drop in micro cross-flow heat exchanger." *Applied Thermal Engineering* 27, (2007) 877-885.

14. Park, H.S. and Punch, J. "Friction factor and heat transfer in multiple Microchannels with uniform flow distribution." *International Journal of Heat and Mass Transfer* 51, (2008) 4535-4543.

15. Hrnjak, P. and Litch, A.D. "Microchannel heat exchangers for charge minimization in air-cooled ammonia condensers and chillers." *International Journal of Refrigeration* 31, (2008) 658-668.

16. Cao, H., Chen, G., and Yuan, Q. "Testing and design of a microchannel heat exchanger with multiple plates." *Ind. Eng. Chem. Res.* 48, (2009) 4535-4541.

17. Jokar, A., Eckels, S.J., and Hosni, M.H. "Single-phase flow in meso-channel compact heat exchangers for air-conditioning applications." *Heat Transfer Engineering* 31, no. 1 (2010) 3-16.

18. Giudice, S.D, Nonino, C., and Savino, S. "Effects of viscous dissipation and temperature dependent viscosity in thermally and simultaneously developing laminar flows in microchannels." *International Journal of Heat and Fluid Flow* 28, (2007) 15-27.

19. Stignor, C.H., Sunden, B., and Fahlen, P. "Liquid side heat transfer and pressure drop in finned-tube cooling-coils operated with secondary refrigerants." *International Journal of Refrigeration* 30, (2007) 1278-1289.

20. Wang, L. and Liu, F. "Forced convection in slightly curved microchannels." *International Journal of Heat and Mass Transfer* 50, (2007) 881-896.

21. Steinke, M.E., Kandlikar, S.G., Magerlein, J., Colgan, E. and Raisanen, A. "Development of an experimental facility for investigating single-phase liquid flow in microchannels." *Heat Transfer Engineering* 27, no. 4 (2006) 41-52.

22. Khan, M.G. and Fartaj A. "Experiments of ethylene glycol-water mixture in multi-port circular straight microchannel slab." *Proceedings of the Society of Automotive Engineers (SAE) World Congress 2010* , Paper #2010-01-0326, Detroit, MI, USA, April 13-15, 2010.

23. Khan, M.G., Fartaj A. and Ting, DSK. "An experimental characterization of cross-flow cooling of air via an in-line elliptical tube array." *International Journal of Heat and Fluid Flow* 25, no. 4 (2004) 636-648.

24. Khan, M.G., Fartaj A. and Ting, DSK. "Study of cross-flow cooling and heating of air via an elliptical tube array." *ASHRAE Transactions* 111, no. Part-I (2005) 423-433.

25. ASHRAE Standard 111-1988. "Practices for measurement, testing, adjusting and balancing of building heating, ventilation, air-conditioning and refrigeration systems." ASHRAE (1988), Atlanta, GA, USA.

26. AHRAE. "ASHRAE Handbook of Fundamentals." *American Society of Heating, Refrigerating and Air-Conditioning Engineers* Chapter 18, (2001) Atlanta, GA, USA, 2001.

27. ASME. "Air cooled heat exchangers." *An American National Standard, Performance Test Code* (PTC) 30-1991. American Society of Mechanical Engineers (ASME): New York, 1991.

28. Bowman, R.A., Mueller, A.C., and Nagle, W.M. "Mean temperature difference in design." *Transactions of the ASME* 62, (1940) 283-294.

29. Shah, R.K., and Sekulic, D.P. "Fundamentals of Heat Exchanger Design."John Wiley & Sons, NJ 2003.

30. Wilson, E.E. "A basis for rational design of heat transfer apparatus." *Transactions of the ASME* 27, (1915) 47-70.

31. Briggs, D.E., and Young, E.H. "Modified Wilson Plot Techniques for obtaining heat transfer correlations for shell and tube heat exchangers." *Chemical Engineering Progress Symposeum Series (AIChE)* 65, no. 92 (1969) 35-45.

32. Khartabil, H.F., and Christensen, R.N. "An improved scheme for determining heat transfer correlations from heat exchanger regression models with three unknowns." *Experimental Thermal Fluid Science* 5, (1992) 808-819.

33. Editorial. "Journal of Heat Transfer: Policy on reporting uncertainties in experimental measurements and results." *Transactions of the ASME, Journal of Heat Transfer* 115, (1993) 5-6.

34. Editorial. "Journal of Fluids Engineering: Policy on reporting uncertainties in experimental measurements and results," *Transactions of the ASME, Journal of Fluids Engineering* 113, (1991) 313-314.

35. Coleman, H.W. and Steele, W.G. "Experimentation and uncertainty analysis for engineers." John Wiley & Sons, New York, 1989.

36. Kasagi, N., Shikazono, N., Suzuki, Y., and Oku, T. "Assessment of high-performance compact micro bare-tube heat exchangers for electronic equipment cooling." *Proceedings of the 1st International Symposium on Process Intensification & Miniaturization* 2003; University of Newcastle upon Tyne, Aug. 18-21.

37. Kang, S.-W., and Tseng, S.-C. "Analysis of effectiveness and pressure drop in micro cross-flow heat exchanger." *Applied Thermal Engineering* 27, (2007) 877-885.

38. Gnielinski, V. "New equations for heat and mass transfer in turbulent pipe and channel flow." *International Journal of Chemical Engineering* 16, no. 2 (1976) 359-368.

39. Choi, S.B., Barron, R.F., and Warrington, R.O. "Fluid flow and heat transfer in microtubes." *Micromechanical Sensor, Actuator and Systems ASME DSC*. Edited by Choi et al. 32, (1991) 123-134.

40. Dittus, F.W. and Boelter, L.M.K. "Heat transfer in automobile radiators of the tubular type." *University of California Publication in Engineering* 2, no. 13 (1930) 443-461.

41. Webb, R. L., and Zhang, M., Heat Transfer and Friction in Small Diameter Channels, *Microscale Thermophysical Engineering*, 2, no. 3 (1998) 189–202.